

Genetically targeted all-optical electrophysiology with a transgenic Cre-dependent Optopatch mouse

Short title: Transgenic Optopatch mouse

Shan Lou¹, Yoav Adam¹, Eli N. Weinstein^{1,4}, Erika Williams², Katherine Williams¹, Vicente Parot¹, Nikita Kavokine¹, Stephen Liberles², Linda Madisen³, Hongkui Zeng³, Adam E. Cohen^{1,4,5,*}

¹ Department of Chemistry and Chemical Biology, Harvard University, Cambridge, MA 02138

² Department of Cell Biology, Harvard Medical School, Boston, MA 02115

³ Allen Institute for Brain Science, Seattle, WA 98107

⁴ Department of Physics, Harvard University, Cambridge, MA 02138

⁵ Howard Hughes Medical Institute

* cohen@chemistry.harvard.edu

Supplementary Online Material

Supplementary Figures S1 – S5

Supplementary Discussion: Heating of brain tissue by 640 nm laser light

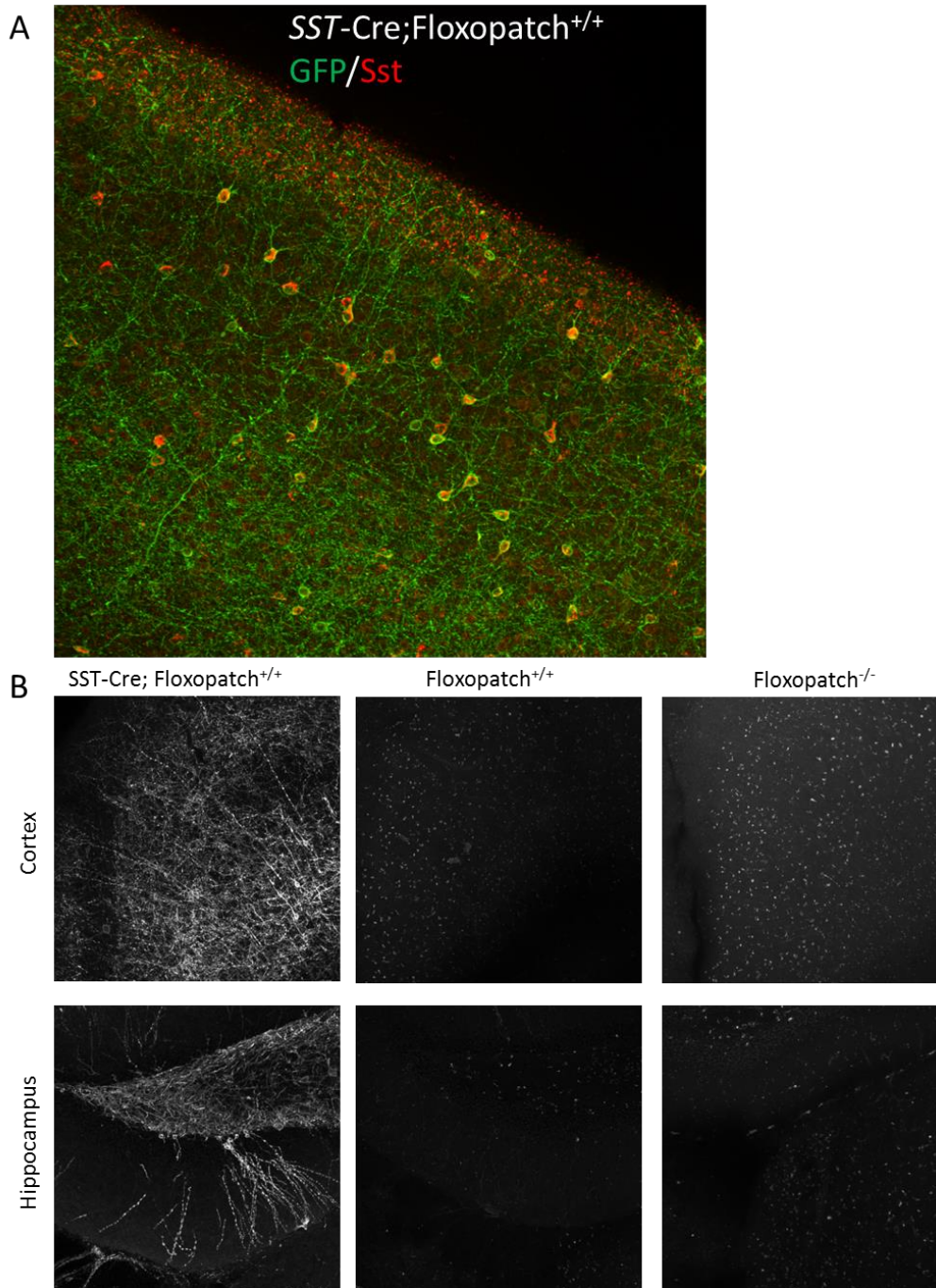


Figure S1. Specificity and selectivity of Optopatch2 expression in Floxopatch mice. A) Confocal image of a fixed brain slice from a SST-Cre^{+/+}; Floxopatch^{+/+} mouse. The slice has been stained with primary antibodies rabbit-anti-GFP and rat-anti-SST, and with secondary antibodies goat-anti-rabbit Alexa 488 and Goat-anti-rat Alexa 647. B) Confocal images of GFP fluorescence in brain slices from animals with and without a Cre driver. The small fluorescent puncta in the Floxopatch^{+/+} images were equally present in the Floxopatch^{-/-} images, suggesting that these came from endogenous autofluorescent particles, rather than from leaky expression.

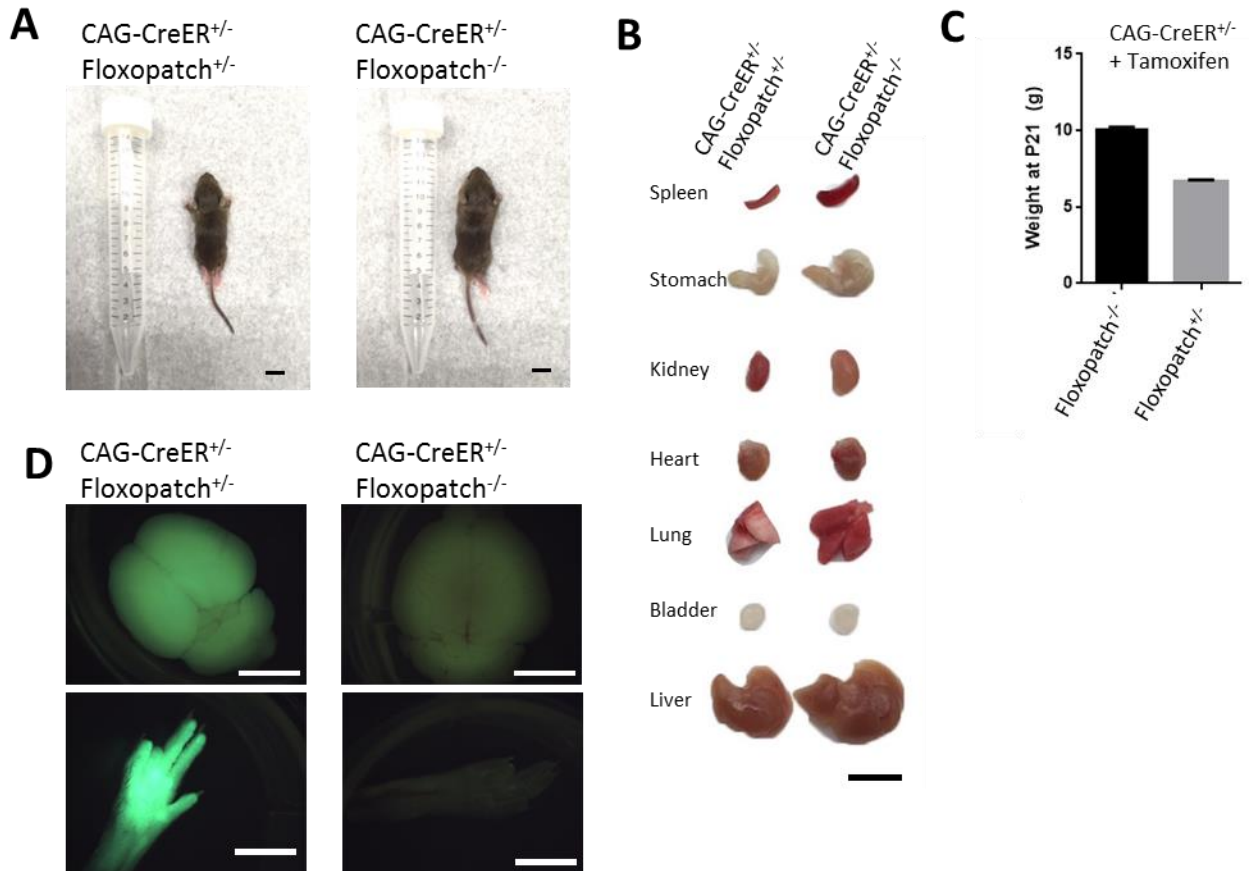


Figure S2. Whole-body expression of Optopatch causes toxicity. **(A)** Comparison of a mouse with whole-body Optopatch expression (CAG-CreER^{+/-}; Floxopatch^{+/-}) and its littermate control (CAG-CreER^{+/-}; Floxopatch^{-/-}). Both were treated with tamoxifen from P15 to P20 and sacrificed on P21. The Optopatch-expressing mouse was smaller in size. Scale bar 1 cm. **(B)** Organs from the mice shown in (A). Organs from mice with whole-body Optopatch expression were smaller than control. Scale bar 5 mm. **(C)** Comparison of the weights of mice with whole-body Optopatch expression and controls. Optopatch-expressing mice were lighter (6.7 g, $n = 3$ Floxopatch^{+/-}, 10.2 g, $n = 2$ Floxopatch^{-/-}). **(D)** Fluorescence images of CheRiff-eGFP, showing Optopatch expression in brain (top) and skin (bottom) of expressing mice and not in controls. Scale bar 5 mm.

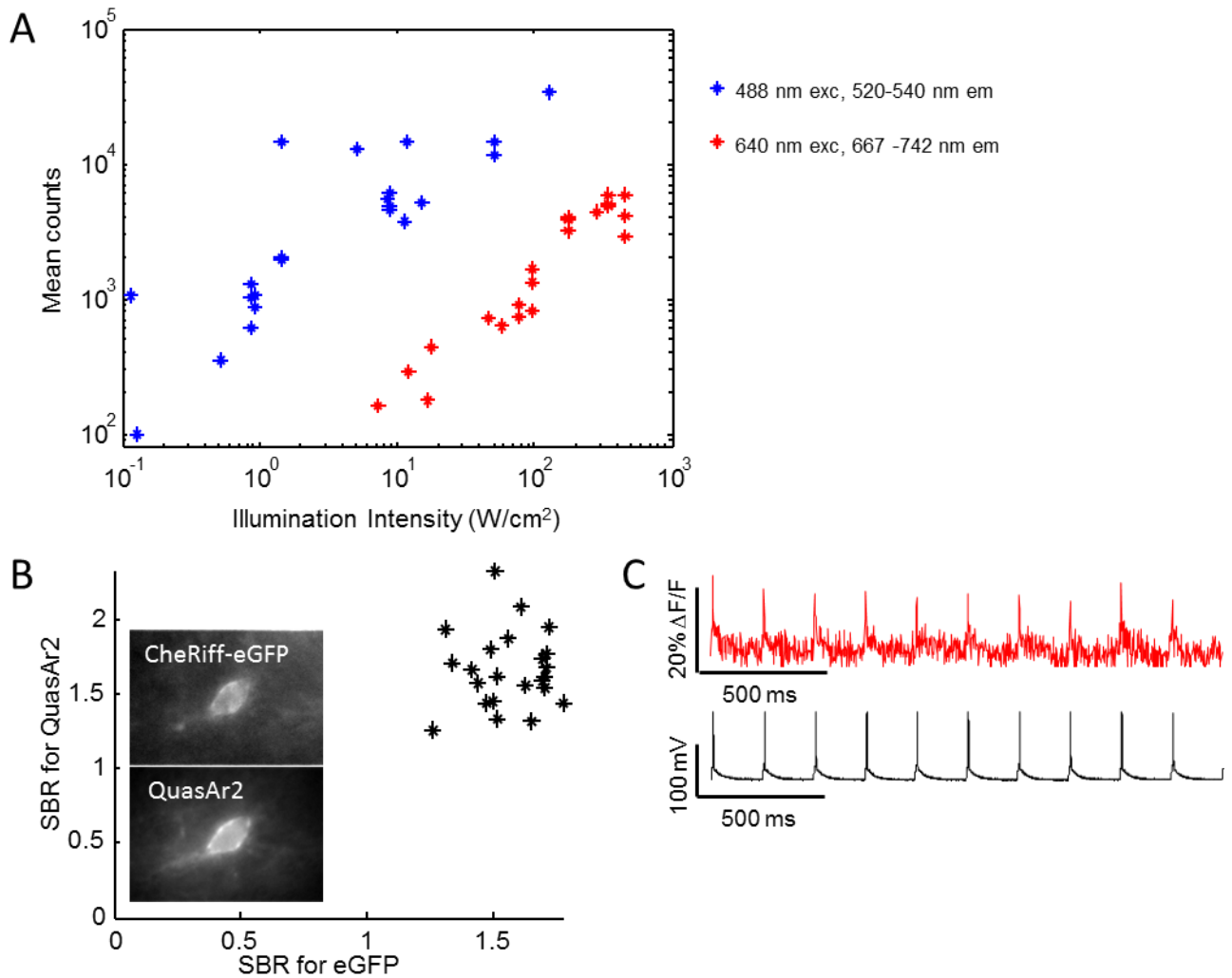


Figure S3. Optical properties of QuasAr2 imaging in acute brain slice. (A) Comparison of tissue autofluorescence under blue excitation (λ_{exc} : 488 nm, λ_{em} : 520 – 540 nm) or red excitation (λ_{exc} : 640 nm, λ_{em} : 667 – 742 nm). Identical illumination spots were established by an iris in the shared excitation path. **(B)** Comparison of signal to background ratio (SBR) between QuasAr2 and eGFP in cells expressing Optopatch2 in acute brain slice. Inset: paired example of QuasAr2 fluorescence and CheRiff-eGFP fluorescence in *CamKII-Cre^{+/-}; Floxopatch^{+/-}* neurons imaged via wide-field epifluorescence in acute brain slice. **(C)** Simultaneous patch clamp and fluorescence measurements in acute brain slice from a *CamKII-Cre^{+/-}; Floxopatch^{+/-}* mouse.

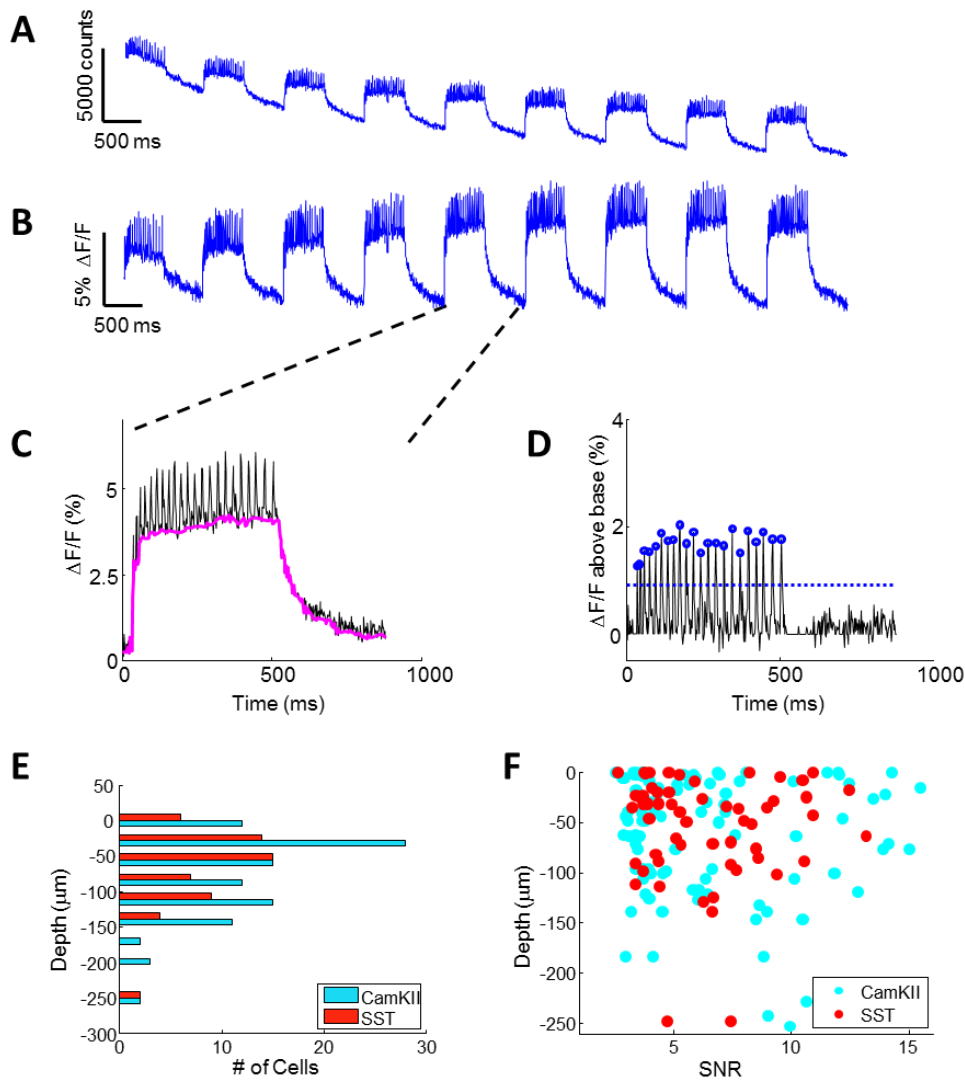
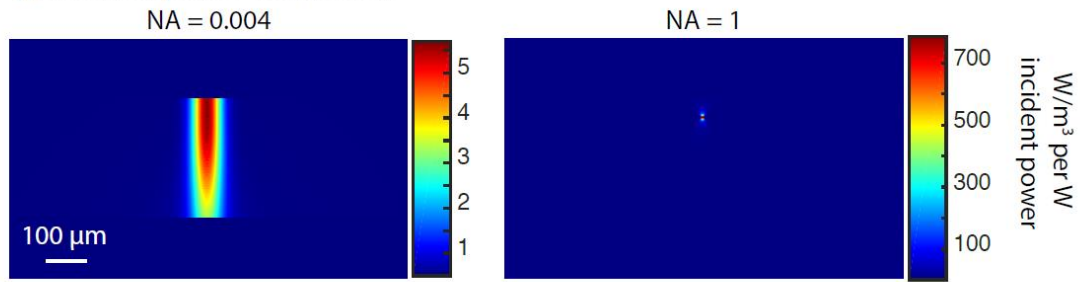


Figure S4. Spike finding in fluorescence recordings in acute brain slice. (A) Raw fluorescence trace from a single neuron with periodic optical stimulation. The decreasing baseline was dominated by photobleaching of the background autofluorescence, and not photobleaching of QuasAr2, as evidenced by the absence of photobleaching in the spike heights. (B) The baseline photobleaching was estimated via a sliding minimum filter and then corrected by division to yield a trace of $\Delta F/F$. (C) Enlarged view showing the local baseline value (pink), estimated via a sliding percentile filter. (D) Signal above baseline; dotted line indicates the dynamically set threshold and blue dots indicate action potential peaks. (E) Depth distribution of recorded cells. (F) Signal-to-noise ratio (SNR) of each cell as a function of depth. Sources with an SNR below 4 were discarded at the start of the analysis.

a) Absorbed power distribution



b) Temperature distribution

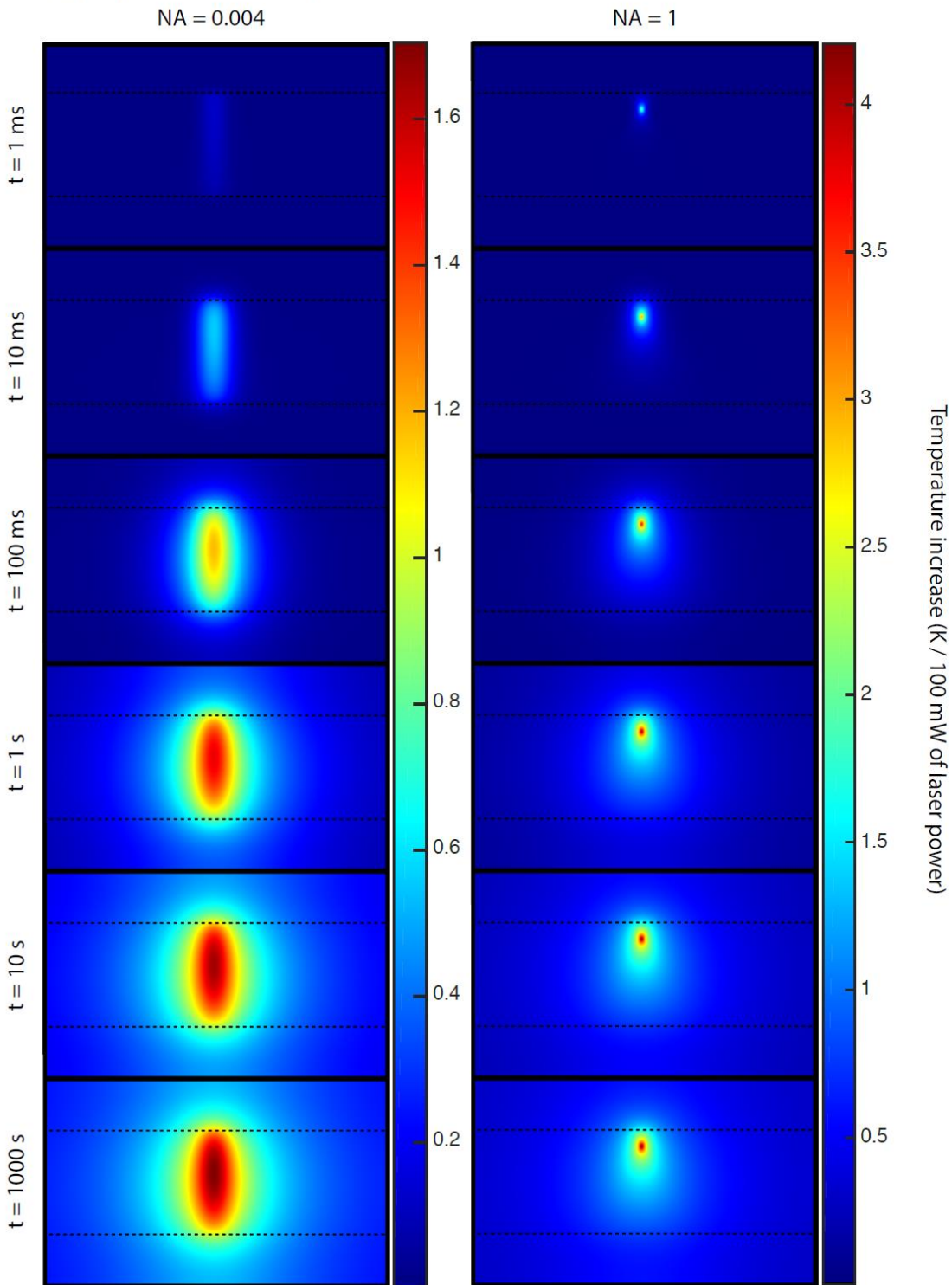


Figure S5. Monte Carlo simulations of laser-induced heating of brain tissue at 640 nm. We performed Monte Carlo simulations of light propagation through tissue, using the Henyey-Greenstein scattering function with an anisotropy of $g = 0.9$. Left: calculation for low NA illumination with a $50 \mu\text{m}$ focal spot. Right: calculation for high NA ($\text{NA} = 1$) illumination. In both cases the focus was $50 \mu\text{m}$ below the surface of the brain slice. We then simulated diffusion of heat using the optical power distribution as the source term. We ignored convective dissipation from blood flow or temperature-dependent changes in metabolic heat production. For a $50 \mu\text{m}$ focus, we calculated a steady-state temperature coefficient of $0.016 \text{ }^\circ\text{C/mW}$, and for a diffraction-limited focal spot we calculated $0.04 \text{ }^\circ\text{C/mW}$. These calculations are in broad agreement with the estimates based on literature simulations and data. To keep temperatures within $2 \text{ }^\circ\text{C}$ of baseline, the laser power should be $< 60 \text{ mW}$.

Supplementary Discussion

Heating of brain tissue by 640 nm laser light

The degree of heating depends not just on the illumination intensity at the focus, but on the total laser power delivered to the sample (how big a region is being imaged), on the duration of the illumination, and on paths for heat removal (blood flow, imaging buffer). Recent reports have studied temperature rises in brain from light delivered via an optical fiber (Stujenske et al., 2015), or near infrared light used in two-photon microscopy (Podgorski and Ranganathan, 2016). Stujenske and coworkers predicted that for 532 nm light exiting a $62 \mu\text{m}$ diameter fiber with an NA of 0.22 , embedded in brain, the maximum temperature rise was $0.4 \text{ }^\circ\text{C/mW}$. Using the data of Jacques (Jacques, 2013), the absorption coefficient at 640 nm is estimated to be ~ 14 -fold lower than at 532 nm . Considering the modest change in scattering length between these two wavelengths, and the fact that the absorption length is much greater than the scattering length, then it is reasonable to approximate the spatial distributions of the light as similar at 532 and 640 nm . The estimated temperature rise at 640 nm is simply the rise at 532 nm , scaled by the ratio of the absorption coefficients. This estimate predicts $0.03 \text{ }^\circ\text{C/mW}$. A power of 40 mW would induce a temperature rise of $1.2 \text{ }^\circ\text{C}$.

Podgorski and Ranganathan studied the temperature rise under near IR illumination in brain tissue. For a 1 mm square scan pattern, they found steady-state temperature coefficients between 0.012 and $0.02 \text{ }^\circ\text{C/mW}$ at wavelengths from $800 - 1040 \text{ nm}$ (less heating at the shorter wavelength). From their reported dependence of temperature rise on scan area, we infer that $\Delta T \sim L^{-0.26}$, where L is the linear dimension of the scan. Scaling their 1 mm scan to a focus of $50 \mu\text{m}$ diameter predicts a temperature coefficient of $0.026 - 0.04 \text{ }^\circ\text{C/mW}$. The absorption coefficient of brain is nearly constant between 640 and 800 nm , so from this calculation we estimate a temperature coefficient at the lower end of this range, $0.026 \text{ }^\circ\text{C/mW}$. This estimate is remarkably similar to the value of $0.03 \text{ }^\circ\text{C/mW}$ estimated independently from the work of Stujenske and coworkers.

References

Jacques SL (2013) Optical properties of biological tissues: A review. *Phys Med Biol* 58:R37.

Podgorski K, Ranganathan G (2016) Brain heating induced by near-infrared lasers during multiphoton microscopy. *J Neurophysiol* 116:1012-1023.

Stujenske JM, Spellman T, Gordon JA (2015) Modeling the spatiotemporal dynamics of light and heat propagation for in vivo optogenetics. *Cell Reports* 12:525-534.